Cruise Report

Geophysical and Geochemical Study of the Australian-Antarctic Discordance

BMRG05 MV

Hobart (Australia) - Perth (Australia)

January 16, 1996 - February 17, 1996

R/V *Melville*

Chief Scientists

Jean-Christophe Sempéré
University of Washington

David Christie
Oregon State University

Accompanying figures for this report can not be found.

Table of contents

I. Scientific Rationale 3

I.1 Objectives of the field program....3
I.2 The Australian-Antarctic Discordance and the isotopic boundary 3
I.3. Summary of preliminary results....5

II The Data 7

II.1 Navigation 7
II.2 Bathymetry and backscatter data 7
II.3 Total field magnetic anomaly 9
II.4 Gravity anomaly data 10
II.5 Seismic data....12

III Characterization of potential drill sites 13
III.1 Preliminary geological observations 13
III.2 Drill site selection 13

IV Geochemical Sampling 14

V Geophysical study of the eastern AAD segments....16
V.1. Bathymetry 16
V.2. Gravity Analysis....19
V.3. Magnetic Field Analysis 20

References....21

Appendices

A.1 Existing data within survey area
A.2 List of Participants
A.3 Scripps' use of the SEGY header
A.4 Bathymetric, sidescan sonar and seismic reflection data over potential drill sites

I. Scientific Rationale

Leg 05 of the Boomerang expedition of the *R/V Melville* departed Hobart, Tasmania on January 16, 1996 to study a region along and adjacent to the Southeast Indian Ridge (SEIR) near the Australian-Antarctic Discordance. The leg terminated in Fremantle, Western Australia on February 17, 1996. This report describes science operations conducted during the leg and presents some preliminary scientific results.

I.1 Objectives of the field program

The scientific objectives of Boomerang 05 were to characterize and determine the tectonic evolution of a pronounced boundary between global scale mantle provinces of the Pacific and Indian Oceans. This boundary is presently located beneath the Australian-Antarctic Discordance (AAD) (Klein et al., 1988), but there is some evidence that it has migrated westward over approximately the last 40 Ma (Pyle et al., 1992, 1995; Lanyon et al., 1995). This project has two, closely related phases. The first phase is primarily intended to locate and characterize an array of potential sites for a proposed Ocean Drilling leg designed to characterize the isotopic boundary between 7-30 Ma. The second phase is a combined geophysical and geochemical survey designed to locate and characterize the boundary from 0-5 Ma.

I.2 The AAD and the Isotopic Boundary

The AAD is a 500-kilometer-long, unusually deep section of the Southeast Indian Ridge, centered between Australia and Antarctica. It is associated with a residual depth anomaly which extends NNE and SSE across the Australian and Antarctic plates, respectively, to the continental margins. The broad, west-facing, V-shape of the depth anomaly suggests a slow westward migration at about 15 mm a^{-1} (Figures I.2.1 and I.2.2; Marks et al., 1990). The depth anomaly intersects the SEIR in the eastern half of the AAD (segments B4 and B3), where axial depths away from transforms are more than 1000 m deeper than "normal". Seismic studies using Rayleigh waves (Forsyth et al., 1987) and S-SS residuals (Kuo, 1993) show that the AAD is underlain by upper mantle which is cooler than normal. Global tomographic inversions (Roult et al., 1994; Su et al., 1994) also reveal regionally fast shear wave velocities from 250 to 550 km beneath the AAD. The difference in upper mantle shear velocity beneath the AAD relative to 'normal' Pacific seafloor has been interpreted by Forsyth (1992) to reflect a difference in melt fraction of 8% (< 2% if melt forms thin films) and a temperature difference of less than 100°C between the two areas. Satellite-derived gravity data, when corrected for bathymetry, are also consistent with a colder thermal structure and regionally thinner crust beneath the AAD (West et al., 1994). Taken together, these studies strongly suggest that the AAD overlies a region of low melt production from mantle that is cold relative to neighboring segments, especially those immediately to the east.

Mid ocean ridge basalts (MORB) from the Indian Ocean are distinct from those of the Pacific Ocean in having higher $^{87}Sr/^{86}Sr$, lower $^{143}Nd/^{144}Nd$, and higher $^{208}Pb/^{204}Pb$, $^{207}Pb/^{204}Pb$ ratios, at a given $^{206}Pb/^{204}Pb$ ratio (Figure I.2.3) These characteristics have been attributed to the widespread dispersal of mantle material with distinctive isotopic characteristics associated with (1) Indian Ocean hotspot compositions, and/or (2) Gondwana lower continental lithosphere, and/or (3) convectively recycled, subducted, altered oceanic crust that has been

mixed into Pacific type upper mantle (e.g., Subbarao and Hedge, 1973; Hedge et al., 1973; Dupré and Allègre, 1983; Hamelin et al., 1985; Hamelin and Allègre, 1985; Hart, 1984; Michard et al., 1986; Price et al., 1986; Dosso et al., 1988; Klein et al., 1988; Mahoney et al., 1989). The widespread dispersal of the Indian MORB isotopic signature has been attributed to the interaction of Gondwana continental lithosphere with the Kerguelen mantle plume during the breakup of Gondwanaland (Storey et al., 1988; Mahoney et al., 1989; 1992).

The boundary between the 'Pacific' and 'Indian' MORB mantle provinces is defined by an abrupt westward decrease in $^{206}Pb/^{204}Pb$ and $^{208}Pb/^{204}Pb$, and an increase in $^{87}Sr/^{86}Sr$ along-axis, accompanied by systematically lower $^{207}Pb/^{204}Pb$ and $^{143}Nd/^{144}Nd$ values, west of the transform offset between Zones B4 and B5, at ~126°E within the AAD; a transition that occurs over a distance <40 km along-axis (Figure I.2.3; Pyle et al., 1992). Such a sharp boundary between two ocean-basin scale, isotopic domains of the upper mantle is unparalleled along the global mid-ocean ridge system. The processes that control the present location and configuration of the boundary between Indian and Pacific MORB mantle are the principal objects of this study.

Of equal, or even greater, significance has been the realization that this isotopic boundary has recently migrated westward. Off-axis samples dredged from 3-4 Ma seafloor in the easternmost AAD spreading segment record the presence of Indian mantle beneath this segment at that time, even though present day lavas from the same segment are derived from a Pacific mantle source. These observations suggest that Pacific mantle has migrated westward at a minimum rate of 25 mm/a for at least the last 4-5 Ma (Pyle et al., 1992). The relationships among the long-term stability of most of the transforms that delineate the AAD, the slow, long-term migration of the depth anomaly, and the apparently quite rapid recent migration of the isotopic boundary are fundamental to our understanding of this complex region. This project focuses on the Indian-Pacific isotopic boundary. Does the recent migration simply reflect perturbations in a boundary that is permanent feature of the AAD? If so, is it related to the stable basin-wide transforms or to the slow-moving depth anomaly? Alternatively, is the migration itself a long-term phenomenon, resulting from mantle inflow from a shrinking Pacific basin since the final separation of the South Tasman Rise from Antarctica about 40 Ma ago? Although this latter suggestion appears to rely on coincidence, the weight of existing geochemical evidence appears to support it (Pyle et al., 1992). Some possible configurations of the boundary are summarized in Figure I.2.4.

In summary, the principal scientific problems that we tried to address during Boomerang 5 are:

Does the observed migration of the mantle boundary represent continuous, long-term westward migration of Pacific mantle into the region between Australia and Antarctica, or is it simply a localized (~100 km) perturbation of a geochemical feature which has existed beneath the eastern AAD through much or all of its history?

Is the isotopic boundary a consequence of the same long-term mantle features and/or processes that have given rise to the AAD or does it presently coincide with the AAD essentially by chance?

Figure I.2.1: Satellite gravity anomaly over the Southeast Indian Ridge (Sandwell and Smith, 1995).

Figure I.2.2: Residual depth anomaly near the Australian-Antarctic Discordance: (a) calculated at UW based on satellite-derived gravity and a sediment isopach grid, (b) from Marks et al. (1990).

Figure I.2.3: **a.b,** Contrasts in the isotopic character of Pacific and Indian MORB along the SEIR in the vicinity of the AAD. (Data of Klein et al., 1988; Pyle et al., 1992, 1995). **c.** Along axis isotopic profiles showing the location of the isotopic boundary.

Figure I.2.4 : Regional map of the SEIR showing the AAD, the locus of the depth anomaly (striped) and the predicted configuration of an isotopic boundary that is migrating westward from the vicinity of the South Tasman Rise.

I.3 Summary of Preliminary Results

Scientific operations during Boomerang 5 were carried out in two related phases. The first phase was devoted to the acquisition of geophysical data in the form of single-channel seismic reflection, Seabeam bathymetry and sidescan data, gravity and magnetics on the north flank of the Southeast Indian Ridge within and east of the AAD. These data will be used to locate and characterize suitable drill sites for our proposed ODP drilling leg which is intended to determine the configuration and history of a the Indian - Pacific mantle isotopic boundary between about 7 Ma and 30 Ma. We were able to locate suitable sites at all 17 of our proposed locations. This unusually large number of potential sites is designed to cover a range of possible locations of the isotopic boundary and to allow the drilling program to respond to chemical data from each hole as it is drilled.

Data were collected along two N-S and one E-W transects (Figure I.3.1). The E-W profile coincides approximately with Anomaly 9 (~ 30 Ma) (Figure I.3.2). This isochron was chosen because it cuts through the trough of the residual depth anomaly near 41°S, and intersects the eastern AAD boundary at a point north of (and therefore older than) its intersection with the residual depth anomaly (Figure I.3.1). This allows us to identify drill sites on either side of this major geophysical feature, which is one possible locus for the isotopic boundary. The eastern N-S transect follows the 135°E meridian from approximately 46.5°S to 42°S, crossing potential locations of a more rapidly migrating boundary. The western N-S transect crosses back and forth between potential sites in zones B4 and B5, designed to characterize a spreading-parallel boundary, before turning east to characterize additional sites spanning a range of migration rates in younger crust of Zone A. Several dredges were attempted during this second N-S transect but none was truly successful (see section IV). Dredging proved to be a reliable sampling tool only on crust younger than 5-7 Ma. These failures demonstrate quite clearly that drilling is the only tool that can obtain samples at a sufficient number of locations, with appropriate spacing, to accurately define the configuration of the isotopic boundary in older lithosphere. The geological characteristics of the different drilling sites that we have identified are discussed in section VI.

The second part of the field program was devoted to determining the location and geophysical characteristics of the Pacific/Indian mantle boundary. To this effect we obtained continuous geophysical coverage on the north flank of westernmost Zone A (1-7 Ma) extending across segments B5 (0-3.5 Ma) and B4 (0-3 Ma). Although dredging in seafloor older than a few million years is a challenge, nineteen of twenty two dredges were successfully completed within the survey region; they will enable us to determine the 0-5 Ma configuration of the isotopic boundary.

Our geophysical study revealed a westward-pointing, V-shaped pair of bathymetric lineaments that intersect at the B5 spreading axis, close to the B5/B4 transform. This is the present location of the isotopic boundary. These lineaments consist of a series of isolated basins,

each of which is 200-400 meters deep and oriented parallel to the spreading axis. The area within this V is also characterized by a marked negative mantle Bouguer anomaly. Similar features on slow-spreading centers represent the migration of non-transform offsets along the axis of accretion. A second, older tectonic boundary is apparent in 2 - 3.5 Ma seafloor, both north and south of the B5 axis. This boundary separates seafloor displaying lineated, axis-parallel abyssal hills from seafloor characterized by elevated blocks often with transform parallel sides. It is irregular in shape, but it increases from west to east in its distance from the B5 axis, again suggesting westward migration. Both these tectonic trends are potential loci for a migrating isotopic boundary, and their early recognition enabled us to obtain samples from an appropriately placed grid of sites.

Finally, a long term distinction between a magmatically robust, eastern sub-segment of B5, and a generally deeper, more tectonically complex western sub-segment has persisted for at least 5 Ma.

Figure I.3.1 Regional map showing Boomerang 05 ship tracks (black line) and residual depth contours (white). Note that the east-west transect at the northernmost point of the ship track crosses the deepest part of the depth anomaly.

Figure I.3.2 Shiptrack in the Boomerang 05 survey area. Phase one transects are N-S along 135˚E and near 128˚E and E-W near 42˚S .

II The data

II.1 Navigation

The primary navigation system for the R/V *Melville* uses Global Positioning System (GPS) collected on "P-Code" GPS receiver. The P-code GPS receiver is a two frequency receiver originally developed for military applications, installed on the R/V Melville during late 1995. P-code receivers are significantly higher accuracy than standard GPS receivers in that collecting two frequencies of data allows correction for atmospheric diffraction, thereby giving a positioning resolution within 5 meters. Fixes from the P-code receiver are recorded every second and smoothed using a second order Gaussian filter with a full-width of 3 minutes. The smoothed values are logged at 1 minute intervals. Excessive speed or course changes are flagged to spot possible navigation errors. After navigation errors have been corrected, the navigation stream is merged with the center beam bathymetry, gravity and magnetics. No navigation errors were encountered during the BMRG05 survey.

The secondary navigation system for the R/V *Melville* also uses GPS navigation collected on a Trimble Model 4000AX receiver. A Trimble model 10X also records position fixes and is located on the bridge. Fixes are recorded every 3-5 seconds and smoothed using a second order Gaussian filter with a full-width of ~3 minutes.

The coverage obtained during leg BMRG05 is shown in Figures II.1.1 to II.1.3.

Figure II.1.1: Track coverage obtained during leg BMRG05 (bold). Coverage obtained during MW8801, West09, and West 10 is shown in gray.

Figure II.1.2: Boomerang 5 tracks in main study area .

Figure II.1.3: Boomerang 5 tracks in regional survey area.

II.2 Bathymetry and backscatter data

Seabeam 2000

The bathymetric survey was conducted with the Seabeam 2000 system installed on the *R/V Melville*. The characteristics of Seabeam 2000 are summarized in the table below. Briefly , Seabeam 2000 ensonifies a 120° swath of seafloor for depths shallower than 4600 m. Each swath consists of 120 beams with an aperture of 1° each. At deeper depths, each swath consists of 91 beams and ensonifies a 90° swath. The system automatically adjusts the ping period as depth changes to obtain the highest possible data density. The SIO Seabeam 2000 installation can also operate in a shallow mode. In the shallow mode (10 to 600 m), the system will output 61 beams with a spacing of 2° between data points. The projector array on the R/V *Melville* contains 28 projector units to form an array with an active length of 4.3 meters along the keel. The hydrophone array contains 84 elements and is approximately 5.3 meters in overall active length.

Depth Range	10 to 11,000 m
Swath Width (to 4600 m)	120°
Swath Width (to 11,000 m)	90°
Transmit beams (for full swath)	1
Transmit beam width (athwartship, -3dB)	100°

Transmit beam width (athwartship, -8dB)	120°
Receive beam width (fore and aft)	15°
Pulse length	2 to 20 ms
Frequency	12 kHz
Pitch	± 7.5°
Roll	±10°

Processing of Seabeam Data and Editing of Bathymetric Artifacts

Bathymetric artifacts were edited using the *mbedit* interactive beam editing program, part of the MBsystem v4.2 package. Editing does not remove data artifacts from the file, but simply flags designated points by changing their sign. Prior to running *mbedit*, raw merged data files were run through the program *sbfix* (part of the SIO processing package) which removed some of the largest data spikes.

Artifacts are often easily identified by their erratic behavior; i.e., sudden changes in depth from beam to beam and/or inconsistency of structure from ping to ping. Good data points should be "supported": a beam data point is supported if it is consistent with the surrounding beams within that ping and the structure it is part of is consistent with the structure of the adjacent pings. The most common artifacts within the Sea Beam 2000 bathymetric data set are dubbed "frayed edges". As the name implies, frayed edges are marked by erratic behavior at the outermost beams. A frayed edge may consist of just the outermost 1 beam or the entire ping, and range in severity from subtle and hardly worth editing to glaringly obvious and data-destroying if not removed. Frayed edges are easily recognized on the real-time contour plot as sets of tight, highly lineated contours at the outer portion of the swath oriented perpendicular to the track direction. Another common class of artifacts are dubbed "center beam ridges". These are generally small, and therefore usually go unedited, but they are persistent and attention needs to be paid to them. Center beam ridges are noticeable in the real time waterfall plot. Grooves are marked by a drop in depth across a small range in beams, usually near the edge of the swath. They persist over the same set of beams across few to many pings, generating a false "groove" in the bathymetry along the track direction. Grooves are often marked by abrupt changes in depth and erratic behavior, but often enough they are smooth or subtle and difficult to detect. The most helpful factor in identifying grooves is that they are almost always on the same set of beams.

Backscatter Data

Backscatter signals from the ensonified seafloor are processed for intensity display in a manner similar to conventional side-scan sonars. Backscatter data are automatically slant-range corrected (true cross-track distance), a feature which is facilitated by the fact that bathymetry is collected concurrently. The data from each ping are processed into 2048 pixels which are equally spaced in the athwartship direction. The graphic recorder is averaged to 1024 pixels and data from several pings are averaged or interpolated to maintain true scaling in the athwartship and along track directions. The intensity data output to the graphic recorder are corrected for water column loss, pulse stretch-out and backscatter variations due to grazing angles. The backscatter data output to tape is corrected for water column loss only. Processing of the full-resolution (12 bit) side-scan sonar data was performed during BMRG05. At the end of the GMT day, the full-resolution sidescan sonar data were extracted from the hourly side-scan files using the program *sbextractss*. This program ray-traces through the water column to construct the sidescan sonar image. Nineteen different sound velocity profiles were used during Boomerang 05. A pixel size of 5 m was selected. The data were then merged with navigation extracted from the corresponding Seabeam files.

II.3 Total field magnetic anomaly

Aboard the R/V *Melville*, the Earth's magnetic field is measured with a Geometrics Model 801 Marine Proton magnetometer towed 310 meters behind the ship (3.6 times the ship length). Assuming a 10 degree dip angle, the magnetometer bottle is located 305 m behind the transom and 53 m below it. Data are collected at 5.5 second intervals and averaged over one minute intervals. The magnetic field anomaly is calculated by removing the International Geomagnetic Reference Field (IGRF) from the total field. The IGRF is computed by calculating the IGRF at four corners of a one degree square and linearly interpolating for each point within the square.

The magnetic data collected during Boomerang 5 were of reasonable quality (Figure II.3.1). Most of the crossover errors were less than 10 nT. Most of the crossover errors larger than 25 nT were obtained in and out of dredge sites and may not provide an accurate representation of the quality of the magnetic data. Older magnetic data are available in this study area from several sources: data from ships of opportunity, such as the Eltanin profiles, using unreliable navigation and recent, well-navigated studies of the AAD (MW8801, WEST10). Since MW8801 data are the densest, we performed a crossover analysis of MW8801 data, as well as one with BMRG05, MW8801, and WEST10. MW8801 data appear unreliable in this analysis (Figure II.3.2). Further, unacceptable crossover errors exist between the 3 surveys (Figure II.3.3). Although removing a constant offset of 180 nT for MW8801 and 60 nT for WEST10 improved the crossover errors, the agreement between the 3 surveys remains poor. Clearly, a better use of existing magnetic data in this region will require a careful evaluation of offsets between the different cruises. Such an evaluation was not performed at sea.

Shipboard Analysis of Magnetic Data:

As a first step in the analysis of the magnetic data on board the R/V *Melville*, we extracted magnetic and bathymetric profiles across the spreading axis and projected them onto a constant azimuth perpendicular to the axis. The observed magnetic field was then forward modeled in the presence of bathymetry. The result of this effort was the determination for each profile of spreading rate. The profiles were modeled by computing the magnetic field induced by a number of individual blocks of constant thickness (0.5 km) and given polarity located at a given depth. Forward models of magnetic anomalies are shown in Figures II.3.4 and II.3.5.

To remove the effects of topography on the magnetic anomalies and to account for the orientation of the field with respect to structures, we inverted the magnetic field in the presence of bathymetry. We used the method developed by *Parker and Huestis* (1974). We gridded the observed magnetic anomaly field and bathymetry, and used them as input to the inverse problem. To keep the inversion solution stable within the bounds of our study area, we filtered out wave-lengths < 4 km and > 500 km using a cosine-tapered band pass filter. The magnetization is assumed to be due to an axially centered dipole and the ambient field is obtained using the IGRF90. We assumed a constant thickness source layer (1 km) following the bathymetry and a constant magnetization in the vertical dimension.

Figure II.3.1: Analysis of cross-over errors in magnetic data collected during Boomerang 5.

Figure II.3.2: Analysis of cross-over errors in magnetic data collected during MW8801.

Figure II.3.3: Analysis of cross-over errors in magnetic data collected during Boomerang 5, MW8801 and West10. Note the large cross-over errors between Boomerang 5 and the previous surveys.

Figure II.3.4: Forward model of magnetic anomalies.

Figure II.3.5: Forward model of magnetic anomalies.

II.4 Gravity anomaly data

Underway gravity measurements were collected for the duration of the cruise using a Bell BGM-3 shipboard gravimeter. On the R/V *Melville*, data are collected every second, a gaussian filter is applied over three minute intervals for smoothing, and data are stored in one minute intervals. Corrections for gravimeter drift are administered with gravity tie-ins at port before and after the cruise. The free air anomaly is calculated by applying the International Gravity Formula 1967 and an Eötvös correction. The International Gravity Formula used is a Chebychev approximation which yields maximum errors of 0.004 mgal:

$$grs67\ (mgal) = 9.78\ 10^{5} \times (1.0 + 5.28\ 10^{-3} \times (\sin(Latitude))^{2} + 2.35\ 10^{-5} \times (\sin(Latitude))^{4}$$

The Eötvös correction is calculated:

$$Eötvös(\ mgal) = 10^{5} \times (2\ \Omega\ V_e * \cos(Latitude) + V^{2}/R_e)$$

where

Ω = Earth angular velocity = $7.29\ 10^{-5}$ (rad/sec)
V_e = Eastern component of velocity (m/sec)
V = Velocity
R_e = Earth radius = 6378135 m.

We found that, during Boomerang 5, gravity data were of generally good quality despite periods of rough weather and significant course and speed changes during dredging operations. This is to a great extent due to the rate at which the bridge negotiated large course changes (10° per minute) and to the improved navigation using P-code GPS. The turning rate is chosen to prevent ship's attitude sensors from being affected adversely by sharp turns. The excellent response time of the gravimeter also aided in producing high-quality data during large course changes associated with dredging operations.

Shipboard Gravity Data Quality

The standard processing sequence for the BGM-3 data involves acquisition of meter counts at 1 sec intervals (1 Hz), conversion to acceleration, despiking, smoothing, decimation to 60 sec (.017 Hz) and latitude and Eötvös correction. The despiking is accomplished with a median filter and the smoothing with a 600 sec gaussian low-pass filter. At this stage the 1 minute gravity data are merged with P-Code GPS navigation, latitude and Eötvös corrections are made, additional data streams are co-registered and underway merge files are written. The 1 sec data have significant power at Nyquist which results in higher frequencies being aliased into the measured signal. The spectrum for the raw data is dominated by a peak at 10 sec - presumably due to ship motion. The 600 sec gaussian low-pass effectively reduces this peak but some high frequency noise is introduced by the Eötvös correction.

Most applications of underway gravity data use spatial rather than temporal dimensions, therefore further processing is done with cumulative distance as the independent variable. At the end of each GMT day, the daily underway merge files are concatenated to produce a single, continuous cruise gravity data file using cumulative distance as the independent variable. Due to sampling operations occurring during the survey, special precautions had to be taken when filtering and smoothing the gravity data. First, to remove on-station times, data values with repetitious cumulative distances were removed, keeping only the last values of position and gravity in a string of equivalent along-track distances. Next, this raw data file was despiked by removing points which differ from the previous along distance by greater than 10 mgal. This file was filtered with a mean value filter having a full width of 1 nm. Within the survey area, further cleaning was performed to ensure clean data acquisition by hand picking the gravity data to remove bad points not removed by the filtering. This was performed using *Matlab* as an interactive, visual tool in a similar manner to *MBedit* of the bathymetric ping data. Generally the filtering algorithm performed very adequately during days when no sampling had occurred. Whenever sampling operations were undertaken, however, we found it necessary to check the results of the filtering. Large ship speed and/or course changes often introduced large spikes or offsets in the data which were not removed by filtering. Numerous filtering algorithms were performed in an effort to minimize the noise introduced by sampling operations including the algorithm of Small, 1994, however it was always found necessary to visually examine the data and hand-pick the bad points to ensure data quality.

Cross-over analysis of the raw, filtered, and hand-picked data was performed, and the results are shown below and in figure II.4.1. Due to sampling operations, standard cross-over analysis programs give unrealistic results since they do not include a test for time intervals as well as distance intervals; this should be corrected in future versions of these programs. We base our cross-over analysis results on the hand-picked data only, as they have significant time intervals between sampling to give realistic cross-over results. Cross-over errors between MW8801, BMRG05, and other available data were not investigated at sea, but they are planned once final gravity ties for BMRG05 are received on land.

Type of Data	Raw Gravity Data	Filtered Gravity	Hand Picked Data
Cross-over Error	0.667 +/- 1.01	1.095 +/- 1.14	2.38+/- 0.78
Number of Points	16007	122	7

A comparison of the filtered and unfiltered data for February 12, 1996 is shown in Figure III.4.2. This day includes underway survey time, as well as two sampling intervals, the first a wax core between 3:30 and 5:30 am, and the second a dredge between 10:45 am and 3:30 pm. The raw gravity data are plotted in the top panel as well as the result of filtering for this day. The filtering does remove significant amounts of noise inherent in the data, however, during large course changes and/or speed changed during on-station times, spikes remain in the post filtered data. Within the main survey box, these points are easily identified and removed. Figure III.4.3 shows the despiking and smoothing associated with the filtering.

Figure II.4.1: Gravity cross-overs for main survey box; grey is raw data, black is filtered data, and hand picked data only at designated crossings is white. Crossing locations of the raw and filtered gravity data are dots, while designated crossing points are stars. Only the designated crossing points are included in the hand picked analysis.

Figure II.4.2 : Gravity Data for February 12th, 1996; an example of combined sampling and underway gravity data acquisition

Figure II.4.3: Raw minus filtered gravity data showing despiking and smoothing of filtering

II.5 Seismic data

Single channel seismic reflection data were acquired during BMRG05 in order to further characterize potential ODP drilling site. The objectives of this aspect of the BMRG05 expedition, specifically, are to establish sediment thicknesses and basement topography, both necessary for planning of drilling operations:

Equipment

The sound sources used in acquisition of seismic data are 2 SSI S80--80 cubic in waterguns trailing the ship from an 80 ft umbilical at a dip angle ~15 ˚. The receiver used is a multi-channel streamer towed behind the ship with the following characteristics:

Streamer: AMG multi channel

2 active sections @ 50 m. long x 1 m hydrophone spacing
2 stretch sections @ 50 m. long
1 weighted section @ ~2 m. long
1 tow lead, length variable--determine from record.

During field operations , the streamer and one of the air guns were towed over proposed targets. The speed of the ship depended on the quality of the data, monitored on real-time profiler. The majority of the seismic survey was at approximately 8.5 knots, with periods of rough weather, or poor returns slowing to 6-7 knots. Shot spacing was approximately 1 shot every 10 seconds.

Data and Gaps

The survey was conducted between 1430 z Jan. 18 to 0540 z Jan. 22, and from 2308 z Jan. 23 to 2305 z Jan. 25. Both digital and analog forms of the data were recorded by a Sun-Sparc 10 devoted to seismic acquisition and analog data recorders. During the first 9 hours of seismic operations only data from every other shot were recorded in digital form. The full data returns were, however, recorded on the annotated analog records, held at UW. All digital data is recorded in Scripps modified SEGY format, a description of which is given in Appendix 3. We recorded 10 seconds of data for each shot during the first 9 hours, reducing to only 9 seconds for the remainder of the survey to avoid overlapping.

III. Characterization of Potential Drill Targets

III.1. Preliminary Geological Observations

Throughout the area proposed for drilling, there is usually very little relief and the sediment cover is surprisingly thin and discontinuous. Sidescan images and seismic profiles reveal that the greatest sediment thicknesses coincide with the shallowest bathymetry. Such areas are separated by narrow valleys, which may be erosional in origin, or by broader regions in which the seafloor is strongly reflective. The ubiquity of Mn oxides in our older dredge hauls suggests that these areas are characterized by the presence of Mn oxide pavements.

Manganese oxide accumulations take three forms. (1) Hard spherical nodules between 5-10 cm diameter, are typically nucleated on sedimentary materials. Hard layers of vitreous luster surround a spherical core of intermixed oxide and sediment; this latter material also forms layers in the outer parts of the nodule. Based on the form of these nodules, we speculate that they formed as concretions within the sediment pile. They may have been collected when a dredge actually dug through unconsolidated sediment, but it is, perhaps, more likely that they are concentrated, by winnowing, at the sediment-water boundary. (2) Composite nodules consisting of several interlocking partial spheres, each about 1 cm diameter, are also typically nucleated on sedimentary material although some contain small rock fragments. Typically they are, at least partially, composed of more friable, powdery Mn oxides, although vitreous layers also occur. Rare fragments of apparently well-preserved basaltic glass were found in nodules of both types. (3) Crusts of Mn oxide vary considerably in density, ranging from highly porous to hard vitreous forms. Some of these crusts appear in some cases to have formed on rock surfaces, while others retain an inner layer of Mn-cemented sediment, suggesting that they have formed at the sediment-water interface.

III.2. Drill Site Selection

Seventeen "generic" drill sites have were listed in our original drilling proposal, to allow for flexibility in the eventual drilling program in response to continuing geochemical input as the program progresses. Based on our survey data, we have selected seventeen actual sites that fulfil the same requirements. We have based our selection primarily on the single channel seismic records and on the Seabeam sidescan data, supplemented by Seabeam bathymetry. At each location, we chose a site where there appears to be a basement reflector, overlain by at least 50 meters of sediment, although sediment thickness is difficult to estimate in many places from the preliminary shipboard records. As processing proceeds onshore, all sites will be reviewed to ensure that there is adequate sediment for efficient drilling.
Site locations are shownin Figure III.1, and the individual data records on which they are based are included in Appendix 4.

Figure III.1 . Locations of proposed drill sites selected on the basis of Boomerang 05 data (stars) shown in relation to the generic sites of the original proposal (diamonds). Diagonal lines represent predicted locations of a boundary migrating at uniform rates of 30 mm a^{-1} (upper) and ~40 mm a^{-1} (lower). Light near-horizontal lines are crustal isochrons at 2 Ma intervals.

IV. Geochemical Sampling

Sampling Objectives

Twenty six dredge sites and two wax core sites were occupied. Results and locations are summarized in Table IV-1 and Figure IV.1. Note that the first dredge number of this leg is seven (BMRG05MV-D07)

The principal objective of the sampling program was to provide a grid of sample sites covering the range of possible configurations of the isotope boundary off-axis. Onshore analysis of these samples is expected to delineate the configuration of the isotopic boundary in oceanic crust out to approximately 6-7 Ma crustal age and, hence, to determine the style and rate of mantle migration during this period. This information will provide essential guidance in the selection of drill sites in older crust. Eighteen sites of this type were completed, of which thirteen yielded usable basalt samples (usable samples are those that appear in hand specimen likely to yield analytical data capable of distinguishing Indian from Pacific mantle). Three sites yielded peridotites and/or gabbros which are of considerable interest in themselves and which may yield isotopic or trace element data relevant to the isotope boundary problem.
A second important objective was to determine whether dredge sampling on older oceanic crust (>5-7 Ma) could be a feasible alternative to a drilling program -- could dredging alone provide adequate samples to delineate the isotope boundary in ocean crust from 10-30 Ma? Six sites of this type were completed, of which five yielded small collections of manganese oxide crusts and nodules. At two sites, some nodules were nucleated on basaltic glass fragments, some of which appear fresh and potentially usable for our geochemical objectives. One of these sites yielded several small samples of highly serpentinized peridotite and another yielded a single small basalt sample. These rock samples are strongly weathered and/or altered and they are unlikely to yield usable analytical data.

A third objective was to obtain a small number of key samples to fill critical gaps in the existing along-axis sample coverage, primarily in segments B4 and B3, which are at the deepest part of the AAD, and for which all existing samples lie slightly outside the axial valley. One of two wax cores devoted to this objective yielded a small amount (2-3g) of basaltic glass, the other appeared to have impacted talus and was not successful. The two dredges, one in B3 and one in B4, both yielded relatively fresh, but not pristine, pillow basalt samples with glass rims.

Results of the Sampling Program

Distant Sites (>7 Ma)

Off-axis dredging proved to be much more difficult than we had anticipated, and proved to be ineffective for crustal ages greater than about 5 Ma. Of the 6 sites attempted on crust of age 7-25 Ma, only 2 recovered basaltic material. Some or all of this material will probably yield useful isotopic ratios if careful chemical procedures are applied, but in no case are we confident that a full suite of reliable geochemical data can be obtained.

At all sites (5 out of 6) where sample was recovered, manganese oxides, either as crusts or as nodules, were the dominant component of the recovered material. We conclude that "hard" basement exposures throughout this region are characterized by the development of Mn oxide

pavements which either cement loose material in place, or shield exposures of basalt in such a way that they cannot be picked up by the dredge.

A further problem with this type of dredging is that "dredgable" sites (a minimum requirement seems to be at least 400 meters of relief over a horizontal distance of no more than one kilometer) are only rarely encountered away from fracture zones. Throughout our survey area, especially in the smooth topography of Zone A, there are very few "dredgable" sites that we did not attempt. Indeed, several of the broadly defined dredge targets listed in our proposals had to be abandoned for want of a suitable target. If sites were more readily available, one might argue that dredging, even with a very low success rate, could be a cost-effective alternative to drilling. Given our inability to sample effectively away from fracture zones during this leg, and the absence of fracture zones from the off-axis regions of zone A, we are convinced that drilling is the only viable means of accurately locating and characterizing the isotope boundary in crust more than 5 Ma.

Closer Sites (1-7 Ma)

A rectilinear grid of dredge sites over the geophysical survey area, as originally planned, proved impossible to obtain owing to the lack of suitable sites. Nevertheless, by using targets of opportunity, we were able to adequately cover the range of possible configurations of the isotope boundary (Figure IV.1). Useful basalt samples were recovered from the majority of sites attempted. Of 18 sites in this age range, 13 yielded usable basalts, many with fresh glass still attached. In addition, 3 sites yielded peridotites and other plutonic samples. Only 3 sites yielded no sample at all.

Zero-Age Sites

With the advent of GPS-based dynamic positioning it has become possible to precisely locate dredges in the deep, narrow axial valleys that characterize segments B3 and B4. This capability was not available on *Moana Wave* in 1988, and our samples from that time were necessarily obtained from the steep, high rift mountains flanking the axial valley. In order to more precisely define the location and nature of the isotopic boundary at zero-age, we were able to successfully complete one dredge station each in the axial valleys of B4 and B3. In both cases pillow basalts were recovered that are fresh, but not pristine -- they are discolored on fracture surfaces by thin Mn oxide coatings and original glass surfaces show some rusty discoloration. One of two wax cores attempted in B4 recovered a small amount of similarly, slightly aged glass. These observations are consistent with our prior experience, here and elsewhere, which suggests that eruptive activity in this type of axial topography is intermittent, presumably reflecting low magma supply rates.

Figure IV.1 Map showing distribution of Boomerang 05 dredges in relation to earlier dredges, seafloor age (lighter, parallel contours) and residual depth (heavier, irregular contours).

Figure IV.2 Schematic map showing Boomerang 05 dredge sites in relation to earlier sites and to possible configurations of the isotopic boundary.

Figure IV.3 Maps of all individual Boomerang 05 dredge sites.

V. Geophysical study of the eastern AAD segments

V.1 Bathymetry

We use the nomenclature of Weissel and Hayes (1974) who refer to the Southeast Indian Ridge east of the AAD as Zone A, and the AAD itself as Zone B. A1 is the westernmost segment of Zone A, and B5 is the easternmost segment of the AAD.

The new Seabeam coverage obtained during Boomerang 5 allows us to determine the recent evolution of the eastern part of the AAD. This is a very important step in understanding the relationship of the geophysical characteristics of the AAD to the isotopic boundary and its migration. Our coverage includes the north flank of the Southeast Indian Ridge in Zone A1 (from 1 Ma to 6.5 Ma), the south flank of B5 out to 2.5 Ma and its north flank to 3.5 Ma , and the south flank of B4 out to 2 Ma and its north flank out to 2.5 Ma (Figure V.1). In this report, we focus on salient tectonic features identified in the new Seabeam coverage (merged with the existing SeaMARC 2 data), using the satellite gravity data of Sandwell and Smith (1995) to extrapolate further off-axis as needed.

Zone A

In Zone A, the area covered includes the likely range of locations of the isotopic boundary given the constraints on its migration history provided by off-axis dredges in B5 and Zone A. Oceanic crust in this area was accreted along segment A1, adjacent to the AAD. The axis of accretion at present is characterized by an axial high at a depth of 3200 m, extending from the eastern bounding transform of the AAD to the 131°E propagator. SeaMARC 2 bathymetry and satellite gravity data show that the northern (outer) pseudofault of the 131°E propagator is southeast of our Seabeam coverage.

The seafloor in the area surveyed consists of long abyssal hills that are 4-12 km wide, 200-600 m high and are truncated by the transform to the west. They trend 100°, which orientation has been maintained for at least the last 6 Ma. Abyssal hills striking 092° are present at the north edge of our Zone A survey in 7 Ma old lithosphere, indicating a counterclockwise change in spreading direction. The ridges are consistently shallower near the transform. This unusual characteristic suggests that they have been formed by magmatic pulses which abut against the transform fault. Curved abyssal hills near 49°10'S, 128°20'E may indicate the trace of an overlapping offset. Except for this occurrence, no tectonic boundary that could be related to a migrating isotopic boundary is apparent. If migration of the isotopic boundary is associated with propagation of an axial discontinuity, then Pacific mantle must have arrived at the eastern AAD boundary either very recently, or prior to 7 Ma.

Segment B5

B5 is the easternmost segment within the AAD. There is a pronounced morphological transition between the axial ridges of Zone A and the axial valleys of the AAD (Figure V.2). The axis in the eastern part of B5 is also transitional in character. It occupies a shallow rift valley, partially filled with a linear volcanic ridge, apparently with a small seamount forming near its mid-point (Palmer et al., 1993). This seamount aligns with a linear chain of six circular volcanoes extending to about 49°30'S on the south flank and with a series of irregular, low edifices that extends at least as far as a small circular seamount near 47°30'S (3.5 Ma) on the north flank of B5. The western half of the B5 axis is located within a much deeper (1500m) rift valley. The change in morphology is abrupt and associated with a distinct, ridge-normal trace in the abyssal hills on

the flanks of B5 (see below). Basalts with transitional isotopic and geochemical compositions identified by Pyle et al. (1992) are only known to occur within the western axial valley.

The new Seabeam coverage allows us to study the evolution of B5 over the last 4 Ma. Examination of the off-axis data allows us to identify three distinct tectonic boundaries: a N-S boundary dividing the more magmatically robust eastern part of B5 from the western part; a V-shaped pair of lineaments, symmetrical about the axis, that extend across B5 from their intersection with the axis at the B5/B4 transform; and an older, more irregular boundary between axis-parallel abyssal hill terrain and older, more blocky and irregular topography farther from the axis. It is possible that the isotopic boundary coincides with one or a combination of these boundaries.

There has been a fundamental division between the eastern and western subsegments of B5 since at least 5 Ma. A succession of high, axis-parallel abyssal hills in B5 east suggests that this subsegment has been magmatically robust throughout the last 5 Ma, in contrast to B5 west, which has had a much more complex history. Aeromagnetic data (Vogt et al., 1984) confirm the presence of a small offset in mid-segment from 4 to 7Ma. Satellite gravity data indicate the presence of a linear trough 180 km (4.5 Ma) south of the B5 axis, aligned wih the east-west boundary within B5. This trough appears to be the trace of the former eastern boundary of the AAD, 6-7 Ma ago, although the lack of a symmetric counterpart to this feature along the fracture zone north of the axis indicates a complex history in the configuration of the spreading center.

A west-pointing, V-shaped string of isolated, *en echelon* basins is arranged approximately symmetrically about the rift axis. The apex of this V is near the intersection of B5 with the B5/B4 transform and coincides with our present estimate of the westernmost position of the isotopic boundary and so this boundary seems likely to be a surficial manifestation of the isotopic boundary. Similar off-axis traces mark the migration of non-transform offsets along the slow-spreading Mid-Atlantic Ridge, and we interpret this trace as reflecting the migration of a segment boundary across B5. The staggered spacing of the isolated basins corresponds to the spacing of abyssal hills and seamounts in the magmatically-robust eastern half of B5. This suggests that migration may have resulted from repeated E-W propagation of progressively stronger magmatic pulses acoss B5 from the eastern sub-segment. Migration must have begun approximatively 1.5-2.0 Ma ago, but it is unclear whether it originated at the eastern transform or within B5 east. The orientation of this boundary suggests a migration rate of approximately 45 mm a^{-1} , within the range allowed by the sparse existing off-axis samples and consistent with predictions based on an assumption of constant Pacific mantle flow since separation of the South Tasman Rise from Antarctica at ~40 Ma (Pyle et al., 1992).

In B5 west, a symmetric arrangement of abyssal hills, resembling the rift mountains on the flanks of the Mid-Atlantic Ridge, is observed within 50 km of the axis (< 1.2-1.5 Ma). The morphology of the seafloor changes drastically for ages older than 1.5 Ma. Instead of axis-parallel abyssal hills, we observe blocks of high topography bounded by axis-parallel, axis-perpendicular, and, sometimes, oblique scarps. This morphology indicates a complex interaction with the B4/B5 transform fault which may have been migrating in an east-west sense prior to 1.5 Ma ago. The blocks which are closest to the B4/B5 transform are bounded on their western side by abrupt scarps which are as much as 10 km east of the present location of the transform. The recovery of a suite of plutonic rocks from one of these elevated blocks is consistent with a tectonic rather than volcanic origin for this topography. The coincidence of this off-axis morphological boundary, parallel to the B5 axis, with the possible initiation of the V-shaped trace discussed in the previous paragraph indicates that migration of the discontinuity, and possibly of the underlying Pacific mantle, may have occurred in response to, or been caused by, a reorganization in the configuration of the plate boundary. Note that while this anomalous topography was produced at B5 west, B5 east continued to produce lineated abyssal hills indicative of a normal accretionary process.

Segment B4

Segment B4 is characterized by the same irregular, blocky topography as in the older parts of B5 west. SeaMARC 2 mapping during MW8801 provided only partial coverage of this segment. Because of the complexity of this segment, its location at the axis of the depth anomaly and its proximity to the isotopic boundary, an understanding of its nature and history required additional mapping and sampling. The complexity of this segment is reflected in the fact that aeromagnetic data appear to locate the spreading center in an area where only structures with low reflectivity were mapped with SeaMARC 2. Fresh basalt was dredged from a narrow graben farther south during MW8801 -- this graben was believed at the time to be the likely locus of spreading. Satellite gravity data indicate the presence of a broad rift valley even farther south, at the southern edge of the MW8801 coverage. This valley was identified by Palmer et al., 1993 as a probable spreading axis, and Marks and Stock (1995) suggested that this valley is the location of a recent ridge jump.

The new multibeam data clearly delineate this valley and appear to confirm that it is the current locus of spreading. Gridded shipboard magnetic data also indicate that this valley lies close to the center of the Brunhes magnetic interval, contrasting in this case with the earlier aeromagnetic interpretation. Basalts recovered from this valley are fresh, but not pristine, comparable to those recovered in MW8801 Dredge 22, from a narrow graben, adjacent to the transform farther north. Combined with the strong sidescan reflectivity throughout the area, these samples suggest that erutive activity may occur at more than one location. Seabeam data clearly show a non-transform offset located near 125°30'E, at about the middle of B4. This offset is manifested by a large (7 km) northward jog of the south rift valley wall and by a transform-parallel ridge located north of the axis and aligned with the break in the valley wall. This discontinuity offsets the Brunhes/Matuyama boundary which is well defined in the western part of B4, but not well defined in B4 east.

Seabeam coverage of the north flank of B4 extends to 3.5 Ma in B4 east and to 2.5 Ma in B4 west. Coverage of the south flank extends to 2.5 Ma. The complex off-axis morphology extends almost throughout the north flank of B4. More normal, lineated topography occurs in two small blocks on the north flank, near 49°20'S/125°45'E and near 48°20'S/125°30'E. Two transform-parallel troughs are present north of B4. One lies in continuation of the B3/B4 offset, near 125°35'E, and the other lies near 125°50'E in continuation of the present 125°30'E discontinuity within B4. As in B5, the blocky terrain of B4 suggests a complex interaction between migrating transform/shear zone(s) and ridge-normal extension. In contrast, the lineated abyssal hills south of B4 indicate that the accretionary process has been highly asymmetric with respect to the present axis of accretion. In fact, there does not appear to be a symmetric counterpart for this block of lineatec topography anywhere on the north flank. Satellite gravity data indicate a further complication in this region -- eastward rift propagation appears to have terminated , 130 km north and south of the present B3/B4 offset, about 3 .5 Ma ago. The relationship between this feature and the chaotic topography is unclear at this time. Further analysis of the bathymetric data in conjunction with the constraints provided further off-axis by satellite gravity and those provided by magnetic anomalies will be needed to unravel the evolution of this area.

Figure V.1: Boomerang 5 track coverage superposed on satellite gravity. The age of the seafloor is contoured (Muller et al., 1993). Note that the zero-age contour is offset with respect of the location of the spreading axis accurately represented in the satellite gravity map.

Figure V.2: Bathymetric coverage obtained during Boomerang 5 and merged with SeaMARC II bathymetry.

V.2 Gravity Analysis :

Within the main survey box, the hand picked gravity data were gridded to produce maps of the free-air gravity anomaly (Figure V.2.1) . Mantle Bouguer anomalies were calculated by removing the contribution of the crust/water and crust/mantle interfaces from the free-air anomaly (*Prince and Forsyth*, 1988) (Figure V.2.2). We assumed a constant crustal thickness of 6 km and used values of 1030, 2800 and 3430 kg m^{-3} for the density of sea water, crust, and mantle, respectively. The gravity effects of the crust/water and crust/mantle interfaces were calculated using the method of *Parker* (1972) using a reference level of 3900 meters, equal to the mean depth of the observed bathymetry. The mantle Bouguer correction was subtracted from the free-air anomaly point-by-point along the ship track where we have gravity measurements and these values regridded to produce the mantle Bouguer anomaly map (Figure V.2.3).

The thermal structure and gravity signature due to the cooling lithosphere for the B5 region were calculated using the finite difference method of Phipps Morgan and Forsyth (1988), assuming a reference temperature of 130°C, a thermal diffusivity of 8.5 x 10^{-7} $m^2 \cdot s^{-1}$, a thermal expansion coefficient of 3 x 10^{-5} $°K^{-1}$, and known plate boundary information to produce a passive mantle flow structure for the region. Subtraction of the thermal correction (Figure V.2.4) from the mantle Bouguer anomaly point-by-point along the ship track where data exist results in the mantle residual anomaly which was again regridded to produce the mantle residual anomaly map (Figure V.2.5). Crustal thicknesses were estimated using the mantle residual anomaly assuming that the entire signal results from topography on the moho with a density contrast of 0.6 g/cc (Figure V.2.6). Under this assumption downward continuation of the mantle residual anomaly to a depth of 6 km plus the reference level used in the Bouguer anomaly (3.9 km) results in moho topography. In the downward continuation process signal wavelengths below 25 km were cut to remove unstable components and tapered up to 35 km to minimize "ringing" effects.

Mantle Bouguer lows are associated with both segments B4 and B5. The most pronounced gravity low is centered over B5 east and forms a westward-pointing V-shape. Along a given isochron, the MBA is lower over B5 east and higher over B5 west. This pattern remains upon removal of the gravity field associated with passive mantle upwelling. Such a pattern may arise due to the presence of thicker crust beneath B5 east than beneath B5 west. The residual gravity field is also consistent with the presence of low-density (melt?) material beneath B5 east. The areas of blocky seafloor topography off-axis in B5 west are associated with the lowest residual gravity values in B5. This may be interpreted in terms of anomalously thin (absent?) crust. Such an interpretation is consistent with the recovery of plutonic rocks from dredge 21. Although a circular mantle Bouguer anomaly is present over the B4 axis, this anomaly has a low amplitude. The residual gravity field in B4 does not display the expected bands of high and low gravity values parallel to the spreading direction. The absence of such a pattern indicates that crustal accretion at B4 does not function in a normal sense. Thus, the validity of applying a thermal correction at this site is questionable and will be examined in detail.

Figure V.2.1: Free-Air gravity anomaly map of the main survey box
Figure V.2.2: Bouguer gravity correction of the main survey box
Figure V.2.3: Bouguer gravity anomaly map of the main survey box
Figure V.2.4: Thermal correction map of the main survey box

Figure V.2.5: Mantle residual anomaly map of the main survey box
Figure V.2.6: Derived crustal thickness anomaly map of the main survey box
Figure V.2.7: Mantle Bouguer gravity anomaly on bathymetry within main survey box
Figure V.2.8: Mantle residual anomaly on bathymetry within main survey box
Figure V.2.9: Derived crustal thickness on bathymetry within main survey box

V.3 Magnetic Field Analysis

Shipboard analysis of the magnetic data collected during Boomerang 5 is based on examination and forward modeling of profiles perpendicular to the ridge axis, and on three-dimensional inversion of the data, taking into account the effects of topography (Figures V.3.1 to V.3.10). Both Zone A and segment B5 exhibit relatively simple patterns of magnetic anomalies (Figures V.3.1 to V.3.3). In B5, minor disruptions in the location of anomalies indicate axial discontinuities. In contrast, magnetic anomalies in B4 have low amplitude and exhibit variations which are difficult to match with a normal seafloor spreading process. Although the data set obtained during Boomerang 5 allows us to locate the Brunhes/Matuyama anomaly boundary with confidence south of the axis, there remains some uncertainty in the location of the Brunhes/Matuyama boundary north of the axis close to the B4/B5 transform. Further, discrepancies between the aeromagnetic data and our shipboard measurements require a careful evaluation of the locations of the aeromagnetic profiles before the two data sets can be merged to provide a unique interpretation of the evolution of this region. Forward modeling of magnetic profiles in B5 and Zone A provides estimates for spreading rate variations within the survey area (Figures V.3.4 and V.3.5). These calculations indicate that the half spreading rate for the north flank of Zone A over the last 5 Ma has been on the order of 45 mm a^{-1}, higher than the rate derived from the NUVEL-1A pole. The lack of conjugate profiles in Zone A hinders interpretation of these results in terms of full spreading rate.

Figure V.3.1: Magnetic profiles in Zone A, B5 and B4 obtained during BMRG05.
Figure V.3.2: Existing magnetic profiles in the BMRG05 survey area from Eltanin cruises.
Figure V.3.3: Aeromagnetic profiles over BMRG05 survey area (from Vogt et al., 1984).
Figure V.3.4: Table of spreading rates obtained by forward modelling of selected BMRG05 magnetic profiles.
Figure V.3.5: Forward model of magnetic profiles in (a) Zone A1, (b) B4, (c) B5.
Figure V.3.6: Magnetic field over survey area.
Figure V.3.7: Bathymetric plots showing area of three-dimensional inversion.
Figure V.3.8: Magnetization solution obtained by inversion of the magnetic field.
Figure V.3.9: Topographic contours superposed on magnetization inversion.
Figure V.3.10: Magnetization contours superposed on bathymetry.

References

De Mets C., R. G. Gordon, D. F. Argus, and S. Stein, Current plate motions, Geophys. J. R. Astron. Soc., London, 101, 425-478, 1990.

de Moustier, C. and M. C. Kleinrock, Bathymetric artifacts in SeaBeam data: How to recognize them and what causes them, J. Geophys. Res., 91, 3407-3424, 1986.

Dosso, L., H. Bougault, P. Beuzart, J.-Y. Calvez, and J.-J. Joron, The geochemical structure of the South-East Indian Ridge, Earth Planet. Sci. Lett.., 88, 47-59, 1988.

Dupré, B., and C. J. Allègre, Pb-Sr isotope variation in Indian Ocean basalts and mixing phenomena, Nature, 303, 142-146, 1983.

Forsyth, D. W., R. L. Ehrenbard, and S. Chapin, Anomalous upper mantle beneath the Australian-Antarctic Discordance, Earth Planet. Sci. Lett., 84, 471-478, 1987.

Forsyth, D. W., Geophysical constraints on mantle flow and melt generation beneath mid-ocean ridges, Mantle Flow and Melt Migration Beneath Mid-Ocean Ridges, ed. by J. Phipps Morgan, D. Blackman and J. Sinton, Geophysical Monograph, 71, 1992.

Hamelin, B., and C. J. Allègre, Large-scale regional units in the depleted upper mantle revealed by an isotope study of the South-West Indian Ridge, Nature, 315, 196-199, 1983.

Hamelin, B., B. Dupré, and C. J. Allègre, Pb-Sr-Nd isotopic data of Indian Ocean ridges: new evidence of large-scale mapping of mantle heterogeneities, Earth Planet. Sci. Lett.., 76, 288-298, 1986.

Hart, S. R., A large-scale isotope anomaly in the Southern Hemisphere mantle, Nature, 309, 753-757, 1984.

Hedge, C. E., R. A. Watkins, W. Hildreth, and W. P. Doering, $^{87}Sr/^{86}Sr$ ratios in basalts from islands in the Indian Ocean, Earth Planet. Sci. Lett., 21, 29-34, 1973.

Klein, E. M., C. H. Langmuir, A. Zindler, H. Staudigel and B. Hamelin, Isotope evidence of a mantle convection boundary at the Australian-Antarctic Discordance, Nature, 333, 623-629, 1988.

Klein, E., C. H. Langmuir, and H. Staudigel, Geochemistry of basalts from the SEIR, 115°-138°E, J. Geophys. Res., 96, 2089-2108, 1991.

Kuo, B.-Y., and D. W. Forsyth, Gravity anomalies of the ridge-transform system in the south Atlantic between 31 and 34.5°S: Upwelling centers and variations in crustal thickness, Mar. Geophys. Res., 10, 205-232, 1988.

Lanyon, R. A.J. Crawford and S.M. Eggins, Westward migration of Pacific upper mantle into the Southern Ocean region between Australia and Antarctica, Geology, 23, 511-514, 1995

Mahoney, J. J., J. H. Natland, W. M. White, R. Poreda, S. H. Bloomer, R. L. Fisher, and A. N. Baxter, Isotopic and geochemical provinces of the western Indian Ocean Spreading Centers, J. Geophys. Res., v.94, p.4033-4052, 1989.

Mahoney, J. J., A. P. le Roex, Z. Peng, R. L. Fisher, and J. H . Natland, Western limits of the Indian MORB mantle and the origin of low $^{206}Pb/^{204}Pb$ MORB: Isotope systematics of the central Southwest Indian Ridge (17°-50°E), J. Geophys. Res., in revision, 1992.

Marks, K. M., P. R. Vogt, and S. A. Hall, Residual depth anomalies and the origin of the Australian-Antarctic Discordance zone, J. Geophys. Res., 95, 17325-17338, 1990.

Marks, K. M., D. T. Sandwell, P. R. Vogt, and S. A. Hall, Mantle downwelling beneath the Australian-Antarctic Discordance zone: Evidence from geoid height versus topography, Earth Planet. Sci. Lett., 103, 325-338, 1991.

Marks, K. M. and J. M. Stock, Asymmetric seafloor spreading and short ridge jumps in the Australian Antarctic Discordance, Mar. Geophys Res., 17, 361-373.

Michard, A., R. Montigny, and R. Schlich, Geochemistry of the mantle beneath the Rodriguez TJ and the SEIR, Earth Planet. Sci. Lett., 78, 104-114, 1986.

Palmer, J., J.-C. Sempéré, J. Phipps Morgan, and D. Christie, Morphology and tectonics of the Australian-Antarctic Discordance, Mar. Geophys. Res., 15, 121-152, 1993.

Parker, R. L., The rapid calculation of potential anomalies, Geophys. J. R. Aston. Soc., 31, 447-455, 1972.

Parker, R. L. and S. P. Huestis, The inversion of magnetic anomalies in the presence of topography, J. Geophys. Res., 79, 1587-1593, 1974.

Price, R. C., A. K. Kennedy, M. Riggs-Sneeringer, and F. A. Frey, Geochemistry of basalts from the Indian Ocean triple junction: Implications for the generation and evolution of Indian Ocean ridge basalts, Earth Planet. Sci. Lett., 78, 379-396, 1986.

Pyle, D. G., D. M. Christie, and J. J. Mahonney, Resolving an isotope boundary within the Australian-Antarctic Discordance, Earth Planet. Sci. Lett., 112, 161-178, 1992.

Pyle, D. G., D. M. Christie, J.J, Mahoney, and R. A. Duncan, Geochemistry and geochronology of ancient southeast Indian and southwest Pacific seafloor, J. Geophys, Res., 100, 22261-22282, 1995.

Roult, G., D. Rouland, and J.-P. Montagner, Antarctica II: Upper mantle structure from velocities and anisotropy, Phys. Earth. Planet. Int., 84, 33-57, 1994.

Sempéré, J.-C., J. Palmer, D. Christie, J. Phipps Morgan and A. Shor, The Australian-Antarctic Discordance, Geol., 19, 429-432, 1991.

Su, W.-J., R. L. Woodward, and A.M. Dziewonski, Degree 12 model of shear velocity heterogeneity in the mantle, J. Geophys. Res., 99, 6,945-6,980,

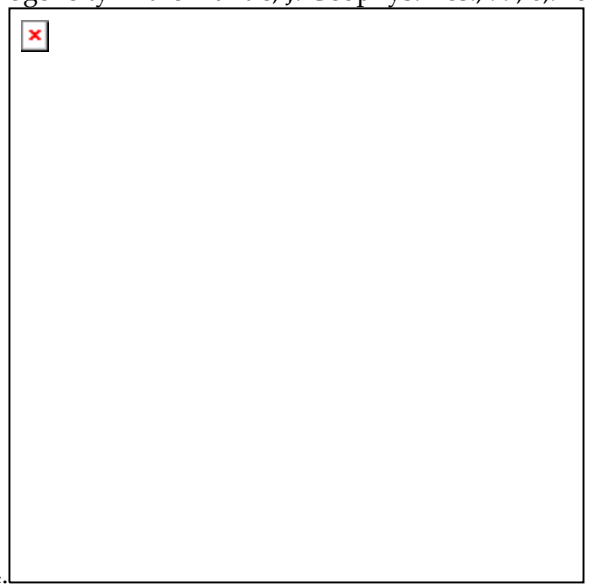

1994.

Storey, M., A. D. Saunders, J. Tarney, I. L. Gibson, M. J. Norry, M. F. Thirlwall, P. Leat, R. N. Thompson, and M. A. Menzies, Contamination of Indian Ocean asthenosphere by the Kerguelen-Heard mantle plume, Nature, 338, 574-576, 1989.

Subbarao, K. V., and C. E. Hedge, K, Rb, Sr and $^{87}Sr/^{86}Sr$ in rocks from the Mid-Indian Ocean Ridge, Earth Planet. Sci. Lett., 18, 223-228, 1973.

Vogt, P. R., N. Z. Cherkis, and G. A. Morgan, Project Investigator-I: Evolution of the Australia-Antarctic Discordance deduced from a detailed aeromagnetic study, in Antarctic Earth Science, Proceedings 4th Int. Symp. on Antarctic Earth Science, edited by R. L. Oliver, P. R.

James and J. B. Jago, pp. 608-613, Australian Academy of Science, Canberra,
1984.

Weissel, J. K. and D. E. Hayes, The Australian-Antarctic Discordance: New results and implications, J. Geophys. Res., 197, 2,579-2,587, 1974.

West, B. P., J.-C. Sempere, D. G. Pyle, J. Phipps Morgan and D. M. Christie, 1994. Evidence for variable upper mantle temperature and crustal thickness in and near the Australian-Antarctic Discordance, Earth Planet. Sci. Lett. 128, 135-153.

Appendix 2

Cruise Participants

Steve Archer
School of Oceanography
University of Washington
Box 357940
Seattle, WA 98195-7940
tel: (206) 543-8956
fax: (206) 543-0275
e-mail: sarcher@ocean.washington.edu

David Christie
College of Oceanic and Atmospheric Sciences
Oregon State University
104 Ocean Admin
Corvallis, OR 97331-5503
tel: (541) 737-5205
fax: (541) 737-2064
e-mail: dchristie@oce.orst.edu

John Huard
College of Oceanic and Atmospheric Sciences
Oregon State university
Oceanography Administration Building 104
Corvallis, OR 97331-5503
tel: (503) 737-
fax: (503) 737-
e-mail: huardj@ucs.orst.edu

Pascal Lecroart
Groupe de Recherche en Géodésie Spatiale
Observatoire Midi-Pyrénnées
18 Avenue E. Belin
31055 Toulouse Cedex
tel: (33) 61332937
fax: (33) 61293327
e-mail: lecroart@goeland.cst.cnes.fr

Matt Niles
College of Oceanic and Atmospheric Sciences
Oregon State university
Oceanography Administration Building 104
Corvallis, OR 97331-5503

Doug Pyle
Dept. of Geological Sciences
San Diego State University
San Diego, CA 92182-1020
tel: (619) 594-3091
e-mail: pyle1@mail.sdsu.edu

Jean-Christophe Sempéré
School of Oceanography
University of Washington

Box 357940
Seattle, WA 98195-7940
tel: (206) 543-0444
fax: (206) 543-0275
e-mail: sempere@ocean.washington.edu

Frank Sprtel
College of Oceanic and Atmospheric Sciences
Oregon State University
104 Ocean Admin
Corvallis, OR 97331-5503
tel: (541) 737-2596
fax: (541) 737-
e-mail: fsprtel@oce.orst.edu

Jeff Standish
Department of Geology
University of Idaho
Moscow, Idaho 83843
Tel:(208)882-5388
e-mail: stand936@uidaho.edu

Brendan Sylvander
College of Oceanic and Atmospheric Sciences
Oregon State University
104 Ocean Admin
Corvallis, OR 97331-5503
tel: (541) 737-2596
fax: (541) 737-2064
e-mail: bsylvand@oce.orst.edu

Brian West
School of Oceanography
University of Washington
Box 357940
Seattle, WA 98195-7940
tel: (206) 543-5156
fax: (206) 543-0275
e-mail: bpw@ocean.washington.edu

Appendix 1

Existing data within the survey area

Geophysical data available from the SEIR near the AAD prior to BMRG05MV consist mostly of individual, widely-spaced lines of shipboard geophysical measurements (Figure I.2.1). The majority of the available data were collected by USNS *Eltanin* in the late 1960s and early 1970s. The *Eltanin* data consist primarily of long, north-south lines at about 5° spacing to the east of 85°E. Data collected by *Eltanin* include bathymetry (single wide-beam), magnetics, gravity and single channel seismic reflection. The gravity and seismic reflection data are generally of poor quality due to severe weather, and are often not usable.

SeaMARC II data were obtained in 1988 during leg MW8801 over the western part of Zone A and eastern part of the AAD (Figure I.2.2). Seabeam bathymetry was obtained along axis between the AAD and the George V Transform during leg WEST08MV and on the north flank of the SEIR across the AAD during WEST10MV (Figure I.2.2).

A dredging program aboard *R/V Vema* in 1975 recovered samples from 11 sites along the SEIR in the vicinity of the AAD (Figure I.2.3). Analyses of these rocks are published by *Anderson et al.* (1980) and *Klein et al.* (1991). Samples were recovered from twenty four dredges during MW8801. Analyses of these samples are reported in Pyle et al. (1992) and Pyle and Christie (submitted).

Figure A1.1: Previous coverage within the Boomerang 5 survey area (from the Lamont data base). Recent multibeam and sidescan sonar studies have been excluded. Regional study area: (a) ship tracks, (b) shiptracks superposed on satellite gravity. Main survey area: (c) ship tracks, (d) shiptracks superposed on s satellite gravity. BMRG05 tracks are shown in bold.

Figure A1.2: MW8801 (SeaMARC 2) and WEST10MV (Seabeam) tracks coverage within Boomerang 5 survey area: (a) Regional survey area, (b) Main survey area. BMRG05 tracks are shown in bold. Coverage obtained during WEST08MV is not shown.

Figure A1.3: Location of dredges recovered from the R/V Vema and during MW8801.